Title:	Plasticity Effects in Incremental Slitting Measurement of Residual Stresses
Author(s):	Michael B. Prime (W-13)
Details:	Engineering Fracture Mechanics, Vol 77, pp. 1552-1566, 2010 http://dx.doi.org/10.1016/j.engfracmech.2010.04.031

Plasticity Effects in Incremental Slitting Measurement of Residual Stresses

Michael B. Prime
Los Alamos National Laboratory
Los Alamos, NM 87545 USA
prime@lanl.gov
voice: +1-505-667-1051
fax: +1-505-665-6333

Abstract

The effect of plasticity is investigated for the incremental slitting, or crack-compliance, method for measuring through-thickness profiles of residual stress. Based on finite element simulations, the errors can be strongly correlated with K_{Irs}, the stress-intensity factor caused by the cut extending into a residual stress field. 3-D simulations also show that the errors are strongly dependent on the amount of constraint provided by the part width. The simulations are used to develop a procedure for estimating errors from experimental data. Even with the possibility of plasticity errors in the measured residual stresses, the K_{Irs} can be simply calculated using only the experimentally measured strains. This K_{Irs} is called "apparent" because the calculation assumes elasticity. The apparent K_{Irs} can then be used to bound the errors in the measured residual stresses. The error bound is given as a function of non-dimensionalized apparent K_{Irs} and part width.

Keywords: Residual stresses, Stress intensity factor, Weight function, Crack compliance.

1. Introduction

1.1. Motivation

The method known most commonly as “crack compliance” but more descriptively called “incremental slitting” or just “slitting” is a unique and valuable tool for residual stress measurement [1]. By incrementally introducing a narrow slit and measuring relaxed strain at each increment of slit depth, it is possible to precisely determine a depth profile of residual stresses. Slitting works well in many situations where other methods are inaccurate, expensive, difficult, or simply not applicable at all. Although sometimes an excellent choice for near-surface stress measurements [2-5], slitting is more unique in its ability to measure through-thickness stress profiles precisely and with excellent spatial resolution. Slitting can be applied to a nearly limitless range of part thicknesses, with results having been reported for layer thicknesses as small as 300 nm [5] and part thicknesses greater 160 mm [6]. Slitting has measured stresses of very low magnitude quite precisely [7-10]. Slitting has measured stresses in parts where diffraction methods could not have been applied to the given material, such as non-crystalline bulk metallic glasses [8, 11], single crystals [12], and polymers [13]. Using electric discharge machining, slitting can be applied to very hard materials [14] where other destructive methods have difficulty with material removal. Other unique applications include functionally-graded materials [15], layered parts [16], ceramics[17], and composites [18].

Because the slitting method relies of the assumption of elastic stress relaxation, plasticity during relaxation can cause errors in the measured stresses. The hole drilling ASTM standard [19] limits the measured stresses to 60% of the magnitude of the yield strength, which is quite limiting since residual stresses, from welding for example, often

exceed that level. Through-thickness slitting has long been assumed to be less sensitive to yielding, but more quantified guidelines must be established.

1.2. Previous Work

Only very limited studies of plasticity in slitting-type measurements have been published. The question of what stress levels would cause plasticity errors in general measurements has not been answered. Residual stresses apparently above yield were measured in pre-cracked specimens and a simple correction for yielding was proposed based on fracture mechanics simulations and some assumptions about the stress field [20, 21]. Another simulation looked at possible plasticity effects in laser peened samples and found the effects to be small even with stresses exceeding the yield strength in a small region [22]. Another simulation considered near-surface measurements of uniform stresses by measuring the relaxed strain between two grooves [23]. Slitting measurements in an autofrettaged thick ring [24] were simulate to investigate possible plasticity errors in some measurements [25]. That measurement involved the slitting of a ring specimen, where the residual hoop stresses across the ring thickness have a large net moment which can lead to a large load on the slit and significant yielding. Plasticity effects when measuring rings could be minimized by first splitting the ring open to measure the net moment and then measuring the remaining residual stresses, which satisfy equilibrium.

1.3. Approach

This study considers a known stress, simulates the measured strains including plasticity effects, back-calculates the residual stresses assuming elasticity, and evaluates

the errors. The study continues on to the subtler problem of identifying errors from only the experimental measurements without any prior knowledge of the stresses.

Two possible yielding scenarios are considered in the study. The first is local yielding in the region near the cut tip where there is a stress concentration. Such yielding is expected to increase with increasing K_{Irs}, the cut-tip stress-intensity factor caused by the cut extending into a residual stress field. This scenario requires addressing 3-D effects because crack tip yielding is considerably smaller for wider specimens where the cut tip is under plane strain conditions. The second yielding scenario is bulk yielding on the surface opposite the cut. When tensile stresses, for example, are relaxed by slitting from one side of a part, the resulting stress redistribution causes a negative change in the stresses on the opposite surface. If and only if the stresses on the opposing surface are opposite sign from the cut surface, this effect potentially leads to yielding underneath the strain gauge.

The three main parameters that are varied in this study were carefully chosen. Parameter studies of plasticity effects on hole drilling [26-30] provide some guidance for this study, but additional considerations must be addressed for slitting. In those studies, the main varied parameter was the magnitude of the residual stresses relative to the material yield strength, which is also varied in the slitting study. The hole drilling studies only considered the measurement of the average, i.e., uniform, stress over the depth of a through-hole [26, 27] or a blind hole [28-30]. The slitting study, however, must necessarily consider the measurement of the through-thickness stress variations by considering different stress profiles, which is the second independent variable. Finally, 3-

D constraint effects must also be examined for slitting, which is the third independent variable. Some hole drilling studies also examined the effect of different levels of strain hardening, which reduces the errors [26, 28, 30]. For this preliminary slitting study, the over-conservatism inherent in assuming perfect plasticity will be accepted. Plasticity in slitting measurements would also be moderated by the width of the slit and the shape of the slit tip. For this study, the slit was conservatively taken as a sharp, zero-width crack.

2. Methods

Finite element (FE) simulations were used to investigate the effect of plasticity on measurements of through-thickness residual stresses in a beam or plate specimen. The strains that would be measured during a slitting experiment were simulated for various residual stress profiles and magnitudes relative to the yield strength. The simulated strains were then used to calculate stresses using a series expansion approach and assuming elasticity. A large parameter study was performed using 2-D plane stress and plane strain simulations. A small number of 3-D simulations were performed to determine the applicability of plane stress or plane strain approximations.

2.1. Geometry and Stress Calculation

Figure 1 shows the standard slitting terminology and geometry for a beam. The models used in this study had a thickness of 1 to normalize other dimensions, so x and a range from 0 to 1 through the beam thickness. Using symmetry, the modeled half-length was 5, which was long enough to eliminate any effect of beam length. It was assumed that the slit did not close during the cutting.

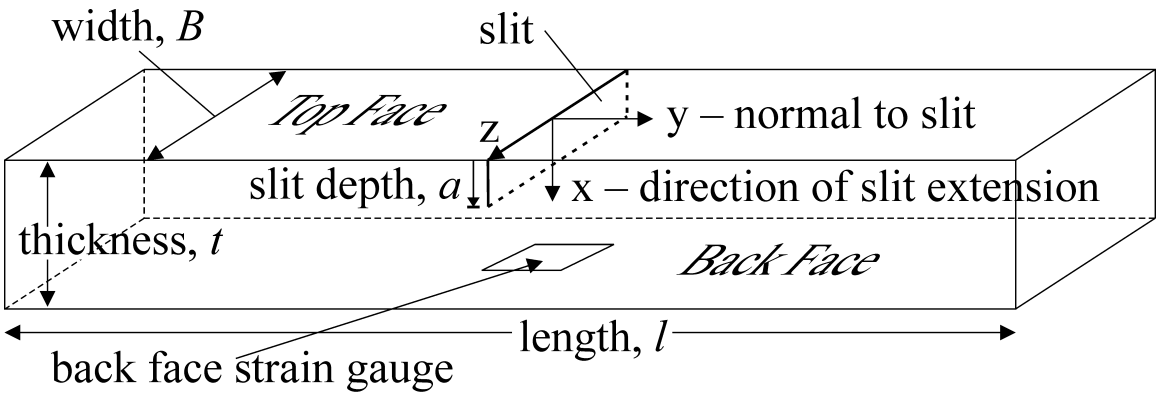

Figure 1. Geometry and coordinate definitions for beam specimen. The gauge measures strains in the y-direction.

The series expansion approach was used to calculate the stresses from the data [31, 32]. Experimentally, at discrete slit depths, a, strains are measured by the strain gauge:

$$\varepsilon(a_i) = \varepsilon_i, \tag{1}$$

where there are m slit depths $i = 1,m$. It is assumed that the stress can be approximated as an expansion of analytic basis functions. For through-thickness measurements, the expansion is commonly taken as

$$\sigma_y(x_i) = \sigma_i \approx \sum_{j=2}^{n} A_j L_j(x_i) = [L]\{A\}, \tag{2}$$

where $L_j(x)$ is the jth order Legendre polynomial expanded with the domain as the full beam thickness. The series expansion begins at $j = 2$ because the zeroth and first order polynomials do not satisfy equilibrium. The first four equilibrium polynomials are shown in Figure 2.

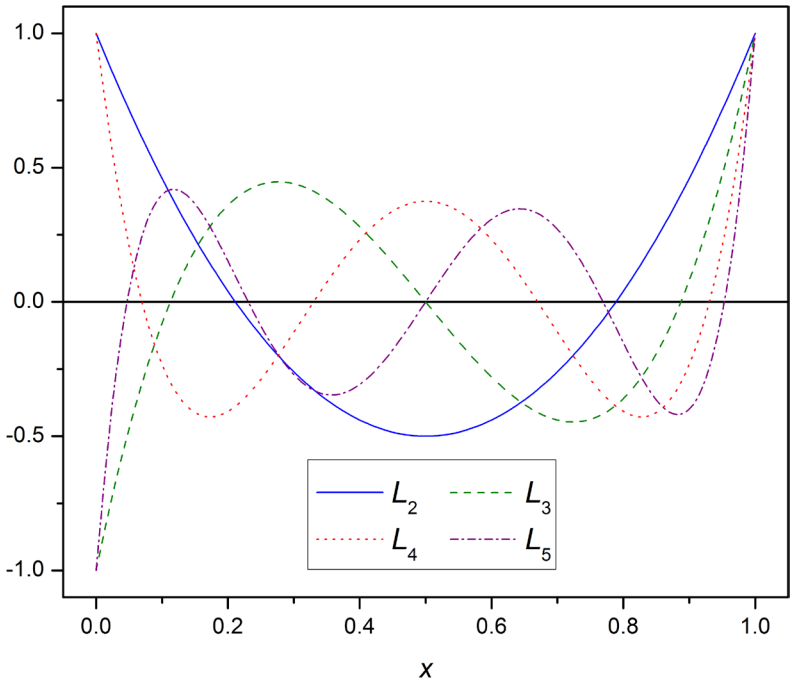

Figure 2. First four equilibrium Legendre polynomials.

The solution for σ now requires choosing an expansion order n and determining the basis function amplitudes A_j . The solution strategy requires determining the strain release $C_j(a_i)$ that would occur at each $a = a_i$ if $\sigma(x)$ were exactly given by each $L_j(x)$. These compliance functions, or calibration coefficients, are usually calculated using finite elements. Using elastic superposition, the strains that would be measured for this approximation of $\sigma(x)$ is then given by

$$\varepsilon_i = \sum_{j=2}^{n} A_j C_j(a_i) = [C]\{A\}. \qquad \textbf{(3)}$$

A least squares fit it used to determine the A_j that provide the best match to the measured strains.

In this study, a conservative assumption about expansion order was made in order to simplify the calculations and the interpretation of results. An objective selection of the expansion order should be made by minimizing the estimated average uncertainty in the

results [33]. In all of the error simulations in this study, the errors increased or remained constant with increasing expansion order. Therefore, the stresses were always calculated using an expansion order of $n = 12$. Expansion orders larger than $n = 12$ are rarely practical and should be used with caution.

2.1.1. Material Behavior

The finite element calculations used incremental plasticity, elastic-perfectly plastic constitutive behavior, the Mises yield surface and the associated flow rule. Isotropic hardening was simulated, so there was no Bauschinger effect. The yield strength was taken as one for all of the simulations, and the magnitude of the initial residual stresses was adjusted to give the desired σ_{max}/S_y:

$$r = \frac{\max(\sigma(x))}{S_y} \quad . \tag{4}$$

The elastic modulus was taken as 1000 to keep the displacements small, and is also realistic since $S_y/E \approx 1000$ for structural metals. Poisson's ratio was taken as 0.3.

2.1.2. Assumed Stress States

Legendre polynomials were initially chosen to represent the possible residual stress profiles. The second order Legendre polynomial, L_2 in Figure 2, was used as a test case for high K_{Irs}, and the third order Legendre polynomial was used as the test case for bulk yielding on the surface opposite the cut. Preliminary calculations demonstrated that higher order Legendre polynomials cause insignificant levels of plasticity.

Based on early results, it was recognized that plasticity effects in slitting were dominated by K_{Irs}, and a more pessimistic test case was constructed. Figure 3 shows the

square stress profile that, for a given peak stress magnitude, results in the theoretically highest K_{Irs}. Such a discontinuous stress profile is physically unrealistic for homogeneous bodies. Therefore, a more realistic stress profile for high K_{Irs} was constructed and is shown in Figure 3. This profile was constructed from Legendre polynomials so that the stresses could be fit exactly by the series expansion process, therefore allowing the study to isolate plasticity errors. Such a residual stress distribution would be most commonly seen with quenching stresses, but quenching stresses rarely exceed half of the yield strength. Such a distribution but with even higher stress magnitudes can be found for the transverse stresses in a butt welded plate [34] or girth welded pipe [35]. Stress profiles giving significantly higher K_{Irs} are increasingly unrealistic.

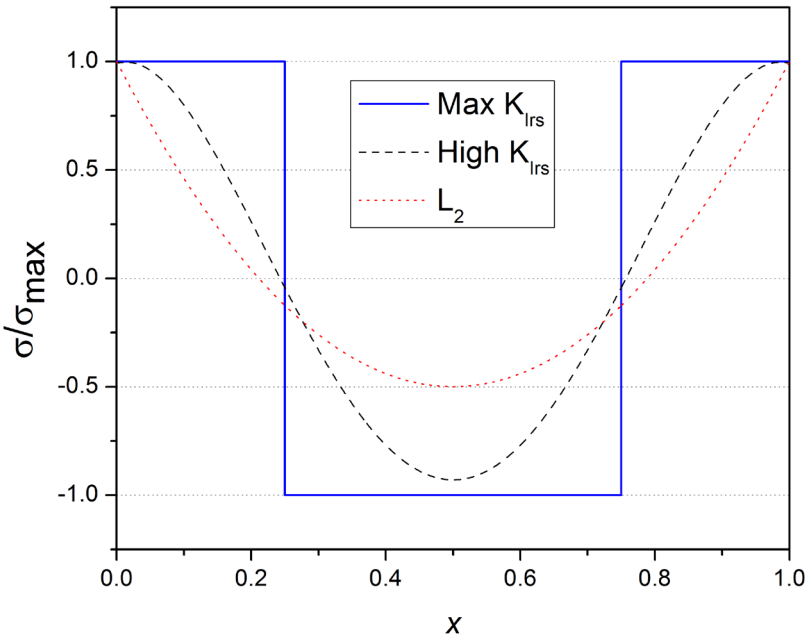

Figure 3. The theoretical stress profile that maximizes $K_{Irs}(a)$, a more realistic stress case to give high $K_{Irs}(a)$, and the 2nd order Legendre polynomial for comparison.

The high K_{Irs} stress profile is given by

$$\sigma = \frac{70}{47}\left[L_2(x) - \frac{1}{3} L_4(x) \right] \qquad (5)$$
$$= -\frac{140}{141}\left(35x^4 - 70x^3 + 36x^2 - x - 1\right)$$

The peak value of 1 is achieved slightly subsurface at $x \approx 0.0145, 0.9855$.

An initial residual stress state throughout the body was modeled. For elastic slitting analyses, it is generally more convenient to use Bueckner's superposition principle and apply pressure loads to the slit faces than to use initial stresses [36]. However, applying pressure loads to an unstressed body only considers the *change* in stress from the slitting, does not include the presence of the initial stresses, and would incorrectly model yielding during relaxation. Away from the cut plane, the initial stresses state was transitioned to zero in order to satisfy both the stress-free surface boundary conditions and equilibrium.

Because the full stress tensor effects yielding, the effect of the transverse stress was considered. The transverse stress σ_z is also commonly of large magnitude and can affect yielding. Besides uniaxial stress, $\sigma_z = 0$, the study considered equi-biaxial stress, $\sigma_z(x) = \sigma_y(x)$, obviously for the plane strain simulations only. The third stress component σ_x is generally smaller because it must be zero on the top and bottom free surfaces, and is therefore ignored in this study.

2.2. Finite Elements

The finite element simulations were carefully constructed to accomplish two main goals: to simulate plasticity as realistically as possible and to isolate the errors caused by plasticity. A zero-width cut was modeled by incrementally removing symmetry boundary conditions in a series of analysis steps. Contact of the cut surfaces was not allowed even

if the surface displaced over the centerline. The residual stresses were simulated by using the initial stress option and an ABAQUS user subroutine `sigini.f [37]`.

2.2.1. Mesh details

The same finite element model was used to simulate the slitting experiments and to calculate the calibration coefficients of Eq. 3. The quadrilateral elements were second order (8-noded, quadratic shape function) in order to better capture stress concentrations and reduced integration for increased accuracy with second order elements as well as reduced computation time. Using symmetry about the cut plane, half of a beam was modeled. The mesh was biased towards the slit region to improve computational efficiency. Along the slit, the elements were squares 0.01 by 0.01, giving 100 elements through the thickness. A convergence study showed that this mesh size was sufficiently converged for stress gradients, and that a cut depth increment of d$a/t = 0.01$ was sufficient to resolve the path-dependent plasticity. The slit was extended to a final depth of $a/t = 0.95$ because deeper cuts are rarely used experimentally. Separate calibration coefficients were calculated for plane stress and plane strain. For 3-D calibration coefficients, the elastic solution for the same mesh is used in order to isolate plasticity effects from other errors, such as the errors from using 2-D compliances for 3-D data [38]. The simulated gauge strain was calculated from the displacement of a node on the beam surface opposite the slit that was 0.035 from the symmetry plane. Dividing this displacement by 0.035 gives the average strain that would be measured by the gauge [39].

To make the 3-D model sizes tractable, the element size was increased to give 50 elements through the beam thickness, and the cut increments were increased to $0.02t$. In

direct comparisons, 2-D simulations using this mesh density were used. A 2-D mesh was then extruded in the z-direction to give a 3-D mesh of reduced integration quadratic shape function (C3D20R) elements. Specimens widths $W = 0.1$, 0.2, 0.5, and $1.0t$ were simulated. Using symmetry, only half of the specimen width was modeled, giving quarter-symmetry models. The elements were equally spaced in the z-direction except for $W = 1.0t$ where a graded mesh was used to keep the calculation tractable. Table 1 shows the details of the 3-D meshes.

Width (B/t)	Elements over half-width	Element width range	Total number of elements
0.1	4	0.0125	28,200
0.2	4	0.0250	28,200
0.5	6	0.0417	42,300
1.0	10	0.0405-0.0607	70,500

Table 1. Mesh details for 3-D FE simulations.

2.3. Fracture Mechanics Calculations

Calculations of the stress intensity factor from extending the crack into the residual stress field, $K_{Irs}(a)$, were made in order to interpret the results. $K_{Irs}(a)$ for the test case residual stresses were calculated using the weight function approach [40]. K_{Irs} was normalized by the yield strength and by the square root of the specimen thickness to provide the appropriate dimensionless parameter for plasticity studies. The normalization by the square root of specimen size becomes clear when one remembers the proportionality between stress intensity factor and global loading is $K_I \propto \sigma\sqrt{a}$ and the crack length will scale with specimen size. In spite of the magnitude of K_{Irs} for a given profile increasing with the square root of the specimen size, plasticity errors do not

depend on specimen size for a given residual stress profile. The extent of the plastic region at a crack tip scales with the square of K_{Irs} and thus will increase linearly with specimen size. The important parameter for plasticity errors is the plastic region size relative to the specimen thickness, which then does not change.

$K_{Irs}(a)$ was also calculated from the slitting strains, as compared to the known stresses, as a method for estimating possible plasticity errors after a slitting test. The calculation from the measured strains [41, 42] is simple:

$$K_{Irs}(a) = \frac{E'}{Z(a)} \frac{d\varepsilon}{da} \tag{6}$$

where $E' = E/(1-\nu^2)$ for plane strain or $E' = E$ for plane stress. For a rectangular beam with $l > 2t$ [43],

$$Z(a) = \frac{-\sqrt{a/t}}{(t-a)^{3/2}} \left(9.7974 - 33.258\, a/t + 73.982 (a/t)^2 - 66.104 (a/t)^3 \right), \tag{7}$$

$$\text{for } \frac{a}{t} < 0.25$$

$$= \frac{-2.532}{(t-a)^{3/2}}, \text{ for } 0.25 < \frac{a}{t} < 1$$

Because the simulated experimental data in this study includes the effects of plasticity, this calculation based on elasticity may not give the exact K_{Irs}; therefore, the result is called the "apparent" K_{Irs}. The strain differential in Eq. 6 was calculated using an exact spline fit. When applying to experimental data, some smoothing of the differential may be required [44]. When applying this calculation to the results of 2D simulations, the E' appropriate to the plane stress or plane strain simulation was used and confirmed to give the correct results. For an experiment that may be somewhere between plane stress and plane strain, the choice is not too important since the difference is only 10% for

$\nu = 0.3$. Nonetheless, using E for $B/t < 0.25$, E' for $B/t > 1.5$, and a linear interpolation in between provided good accuracy based on the 3D simulations in this study.

2.4. Error Calculations

The strain error is the difference between the simulated strain including plasticity, ε_p, and the strains when yielding is not allowed, ε_e. The values are normalized by the maximum strain magnitude from the elastic calculation

$$\tilde{\varepsilon}_{error}(a) = \frac{\varepsilon_p(a) - \varepsilon_e(a)}{\max(abs(\varepsilon_e(a)))} \quad \textbf{(8)}$$

The tilde indicates normalization by a maximum value. The root-mean-square average of this quantity over the cut depths quantifies the average strain error

$$\overline{\partial\varepsilon} = \sqrt{\frac{1}{m}\sum_{i=1}^{m}\left(\tilde{\varepsilon}_{error}(a_i)\right)^2}\,, \quad \textbf{(9)}$$

where m is the 95 cut depths.

While the strain error provides an error measure that is independent of the method used to solve the inverse problem for the stresses, it is the errors in the calculated stresses that are of main interest. The stress error is defined as the difference between the calculated stresses and the known stresses. The stress error is normalized by the maximum of the known stresses.

$$\tilde{\sigma}_{error}(a) = \frac{\sigma_{calculated}(a) - \sigma_{known}(a)}{\max(\sigma_{known}(a))} \quad \textbf{(10)}$$

The root-mean-square average of this quantity over the cut depths quantifies the average error in the calculated stresses:

$$\overline{\partial\sigma} = \sqrt{\frac{1}{m}\sum_{i=1}^{m}\left(\tilde{\sigma}_{error}(a_i)\right)^2} \quad . \tag{11}$$

3. Results & Discussion

3.1. Fracture mechanics

Figure 4 shows the result of the weight-function calculation of $K_{Irs}(a)$ for the test case residual stresses from Figure 2 and Figure 3. The plot ends at $a/t = 0.85$, which is the limit of accuracy for the weight function. The L_2 and high $K_{Irs}(a)$ cases both show a single significant peak that occurs relatively early in the cutting. The peak for the high $K_{Irs}(a)$ is 58% greater in peak K_{Irs} compared to L_2. The L_3 case has two peaks of similar magnitude, with that magnitude another 35% lower than the peak of L_2.

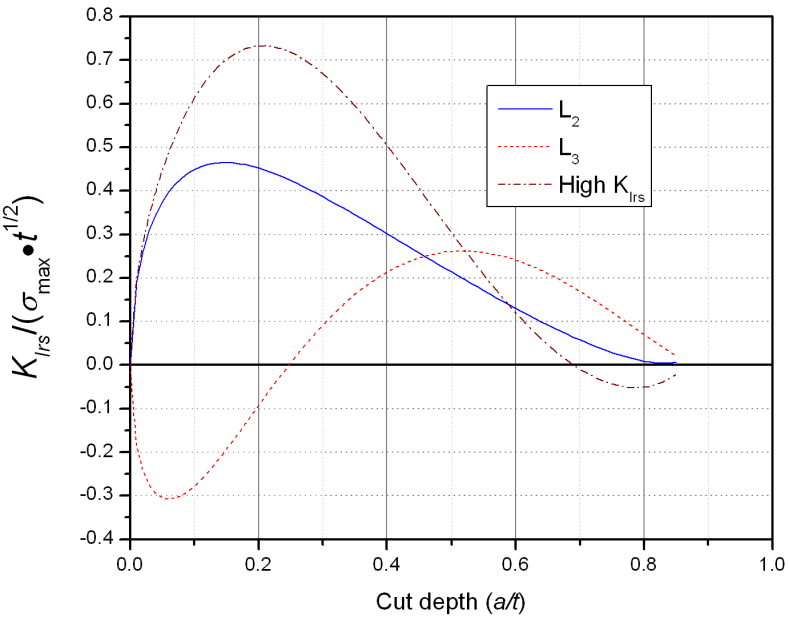

Figure 4. The stress intensity factor from cutting into a residual stress profile corresponding to the test case residual stress profiles.

3.2. Typical results from individual 2-D runs

Figure 5 shows typical simulated slitting strains. For σ_{max}= 0.9 S_y, the strains including plasticity effects are plotted alongside the strains for elastic only behavior for the three test case stress profiles and both plane stress and plane strain. For clarity, only every second data point is plotted. The effect of plasticity is most visible for the plane stress simulations for the high K_{Irs}, and L_2 test cases.

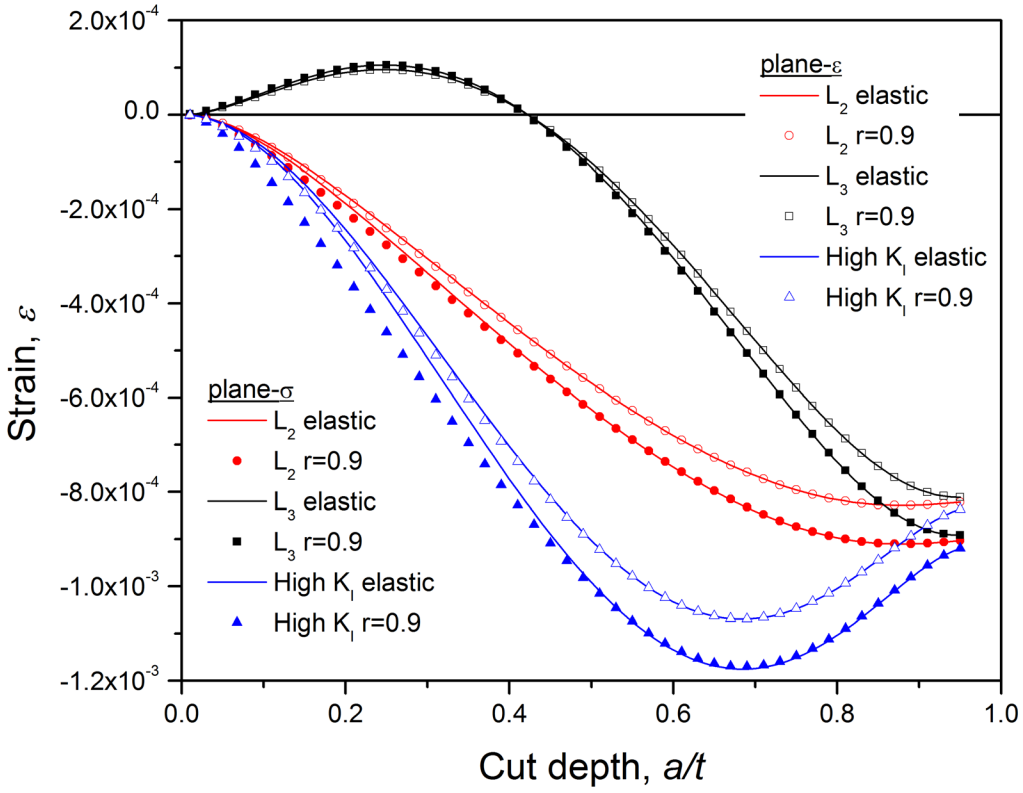

Figure 5. Simulated slitting strains. Lines are elastic strains, symbols are from simulations including plasticity with σ_{max}/S_y = 0.9.

To examine the plasticity effects more closely, Figure 6 shows the strain error of Eq. 8 for the plane-strain L_2 simulation. The strain errors peak at a relatively shallow cut depth, which corresponds with the peak in $K_{Irs}(a)$, Figure 4, as the slit depth is increased. The strain errors return to zero after cut tip plasticity ceases to occur and the remotely

measured strain becomes dominated by the globally released stresses rather than previous local plasticity effects. The magnitude of strain errors scales with stress magnitude.

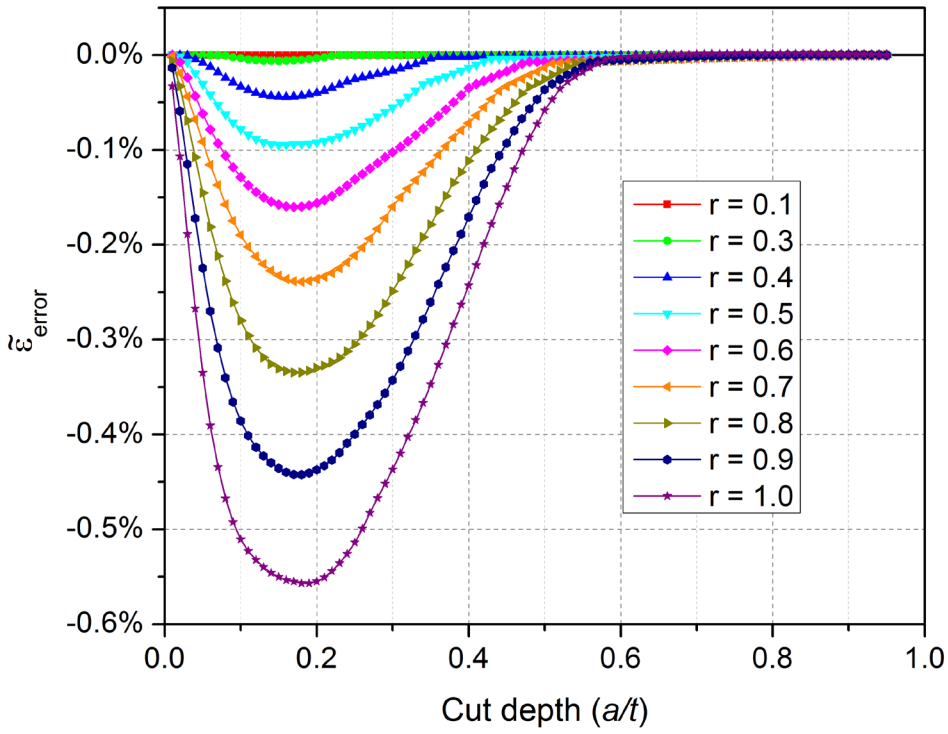

Figure 6. Normalized strain errors for plane strain and L_2 and different levels of $r = \sigma_{max}/S_y$.

Figure 7 shows the L_2 stress errors for the plane strain simulations corresponding to Figure 6, with some of the curves removed for clarity. After calculating the stresses using the 12th order Legendre series expansion, the errors were calculated using Eq. 10. The stress errors are much greater than the strain errors because of the sensitivity of the inverse calculation. The largest stress errors occur near the surface, the location of peak stress magnitudes. The calculated surface stress is most affected by the strains measured at shallow cut depths, which have the lowest magnitudes. The calculated stresses shown in Figure 7 over-predict the actual magnitudes, which aids in recognizing plasticity errors in the stress results.

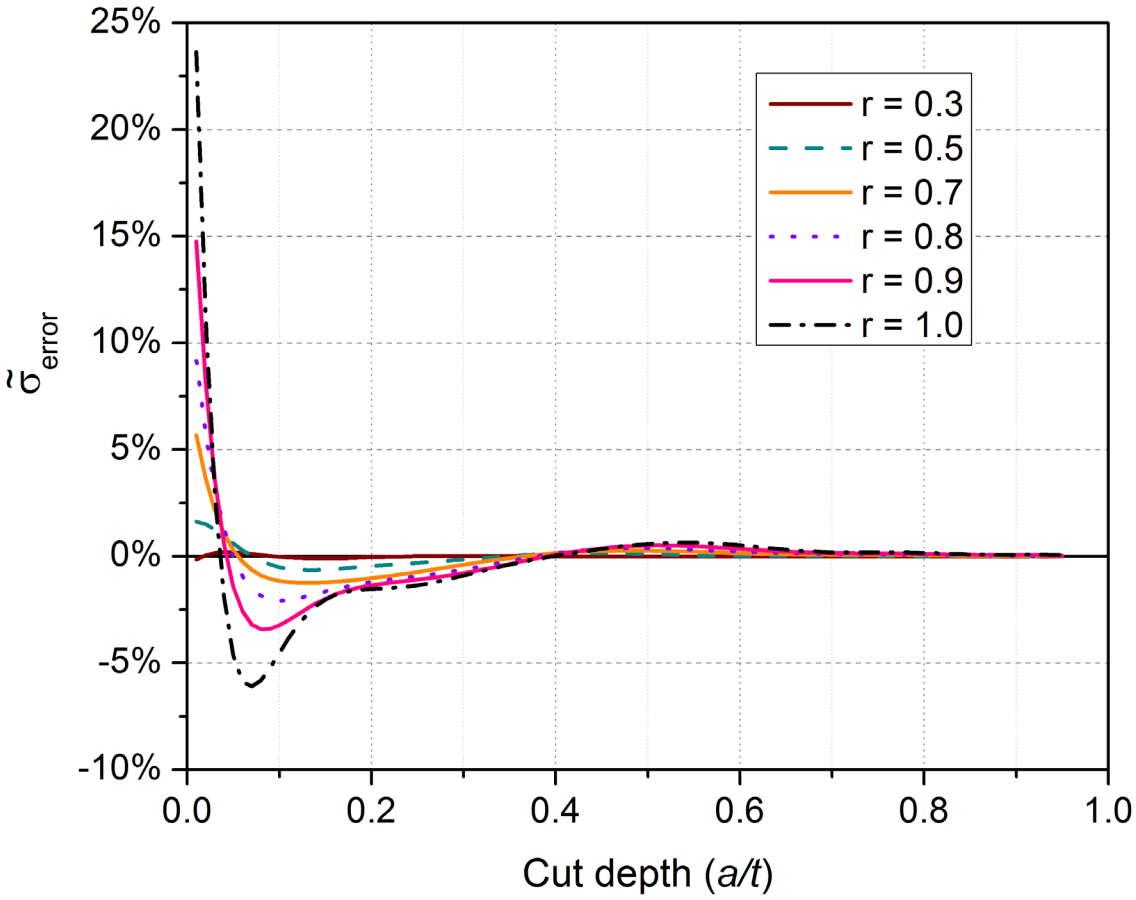

Figure 7. Stress error for plane strain and L_2. The known stress at $a = 0$ is +1, so the maximum errors overestimate the stress magnitudes.

3.3. 2-D Compiled results

Figure 8 shows the average strain errors, Eq. 9, as a function of stress level for the 2-D FE parameter study. The figure represents root-mean-square depth-averaged values of curves including those in Figure 6. As expected, the plane stress simulations show the greatest magnitude of strain errors, often three or four times the level of corresponding plane strain simulations. The high K_{Irs} test case has significantly higher errors than other

profiles. The difference between uniaxial and biaxial stress states is quite small. The L_3 results show a sharp increase above $r = 0.9$ when yielding under the strain gauge occurs.

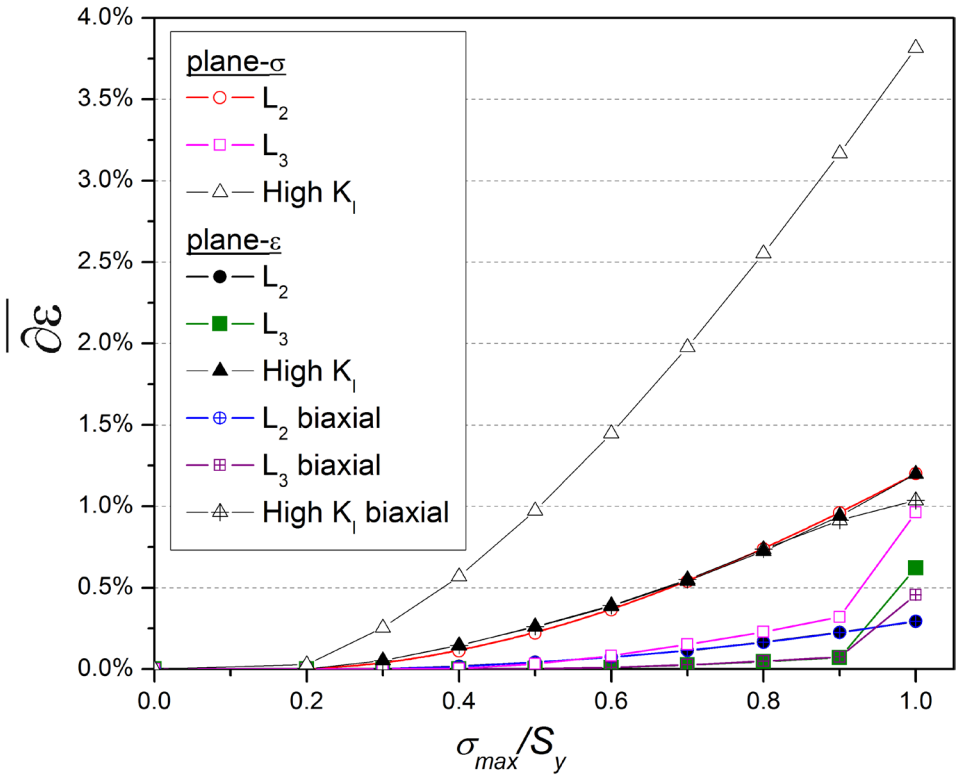

Figure 8. Root-mean-square average strain errors from 2-D runs

Figure 9 shows the average stress errors, Eq. 11, as a function of stress level for the 2-D FE parameter study. The magnitude of stress errors are up to an order of magnitude greater than the strain errors, confirming that the inverting measured strains to original residual stresses magnifies the errors. The errors vary greatly for different stress profiles. Except for the high K_{Irs} profile, the average errors are under 10% for all initial stresses under the yield strength. Similar plots for hole drilling simulations show higher errors (for their single average stress value rather than a depth-average) [28, 29]. The difference between uniaxial and biaxial stresses errors is still insignificant but is larger than in Figure 8 because the shapes of the strain error curves are somewhat different. The

L_3 errors are small even for high stress levels. Furthermore, having near yield magnitude stresses of opposite sign on the two opposite surfaces is already unrealistic. Therefore, the scenario of yielding under the strain gauge is not found to be a realistic error source.

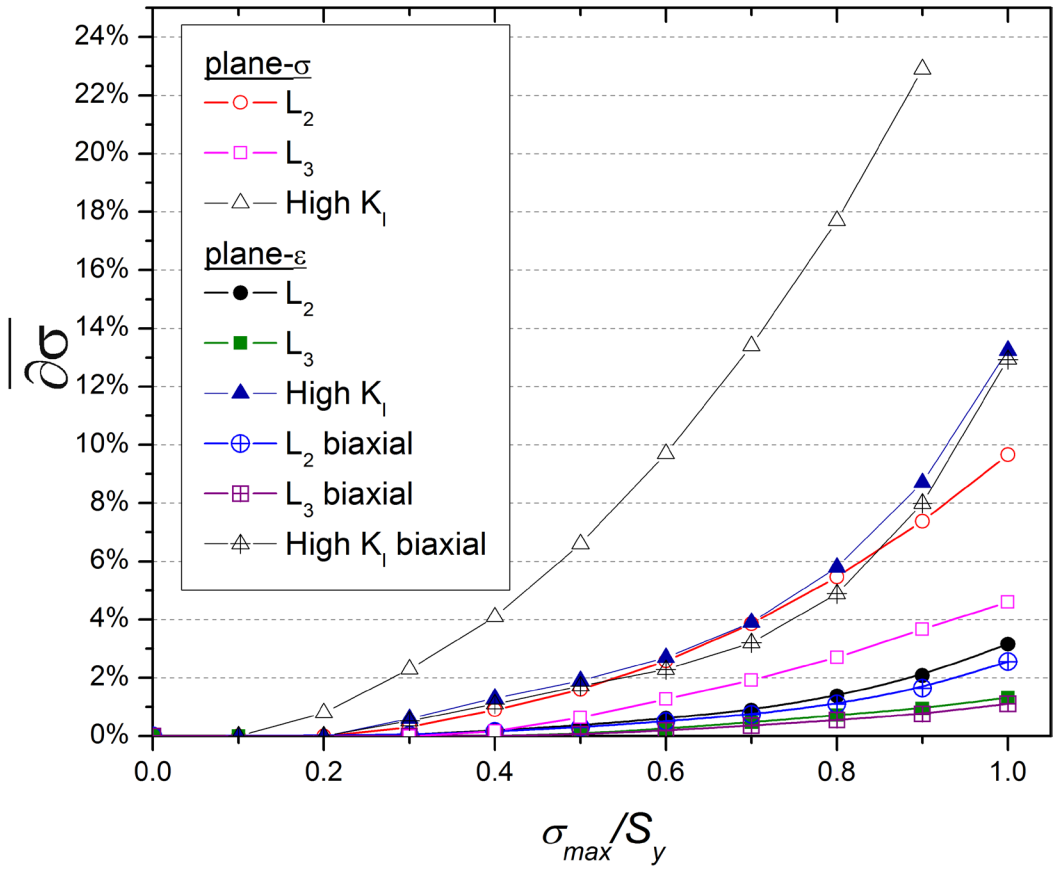

Figure 9. Root-mean-square average stress errors as a function of the peak residual stress relative to the yield strength.

Figure 10 shows that plotting the stress errors versus the peak value of apparent $K_{Irs}(a)$,

$$\hat{K}_{Irs} = \max\left(\frac{K_{Irs}(a)}{S_y\sqrt{t}}\right), \tag{12}$$

gives a much more consistent method for interpreting the results. The stress errors from Figure 9 now collapse into two distinct populations: plane stress and plain strain. The agreement within the populations is striking considering the differences in the stress profiles and especially that the calculated stresses result from the processing of the data through the series expansion inversion process. The difference between the plane strain and plane stress is roughly a factor of three to four, which is consistent with the reduction in plastic zone size because of the triaxial stress state for plane strain.

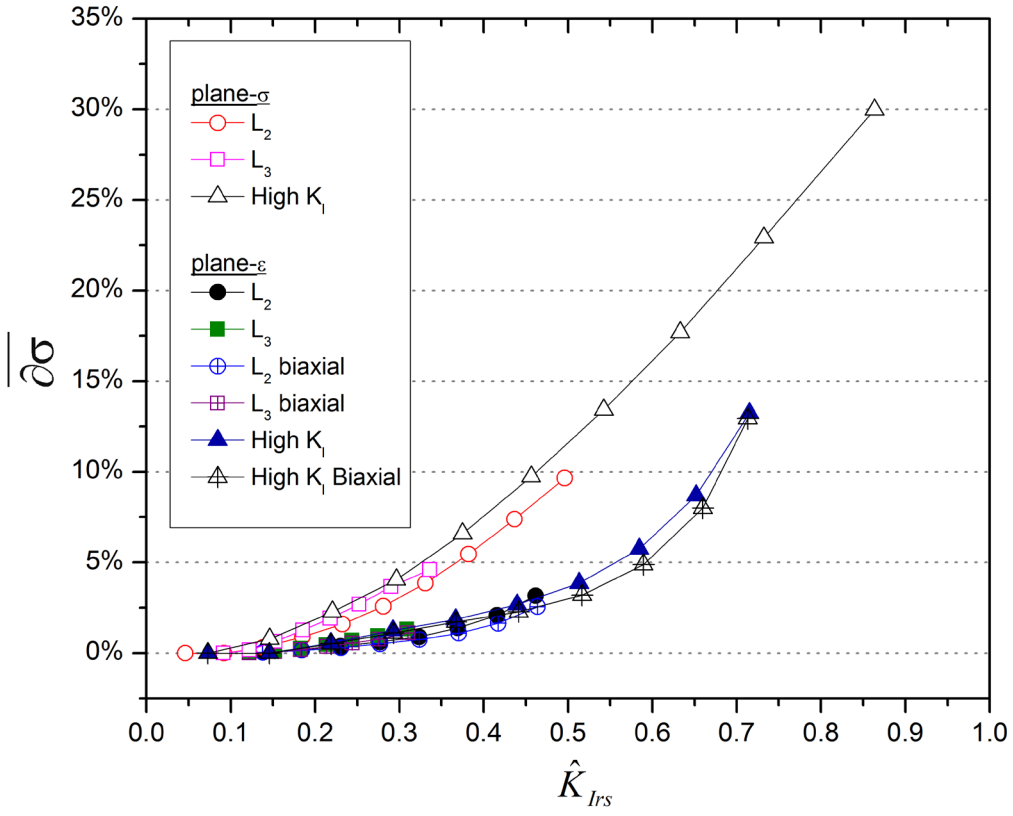

Figure 10. Average stress errors correlate well with the maximum values of the apparent stress intensity factor from the residual stresses.

Figure 11 shows Figure 10 plotted on a logarithmic scale. Near-zero values of error are not plotted. The central regions of the curves show the expected dependence on

the square of K_{Irs}, because that determines the size of the crack-tip plastic zone. For later use in interpolating 3D results, approximate bounding curves are constructed as

$$\begin{aligned} \overline{\partial\sigma} &= 0.46\left(\hat{K}_{Irs}\right)^2 \text{ for plane stress} \\ &= 0.31\left(\hat{K}_{Irs}\right)^{2.6} \text{ for plane strain} \end{aligned} \quad \textbf{(13)}$$

At higher levels of K_{Irs}, the fits to a dependence on the square of K_{Irs} are not as good partly because the apparent K_{Irs} is not as good an approximation to the actual K_{Irs}. The curve for plane strain therefore uses a higher exponent in order to remain conservative for the high K_{Irs} profile with peak stresses over $0.8S_y$. For general reference as threshold values, note that the errors do not exceed even one percent until $\hat{K}_{Irs}$ exceeds about 0.15 for plane stress or 0.26 for plane strain.

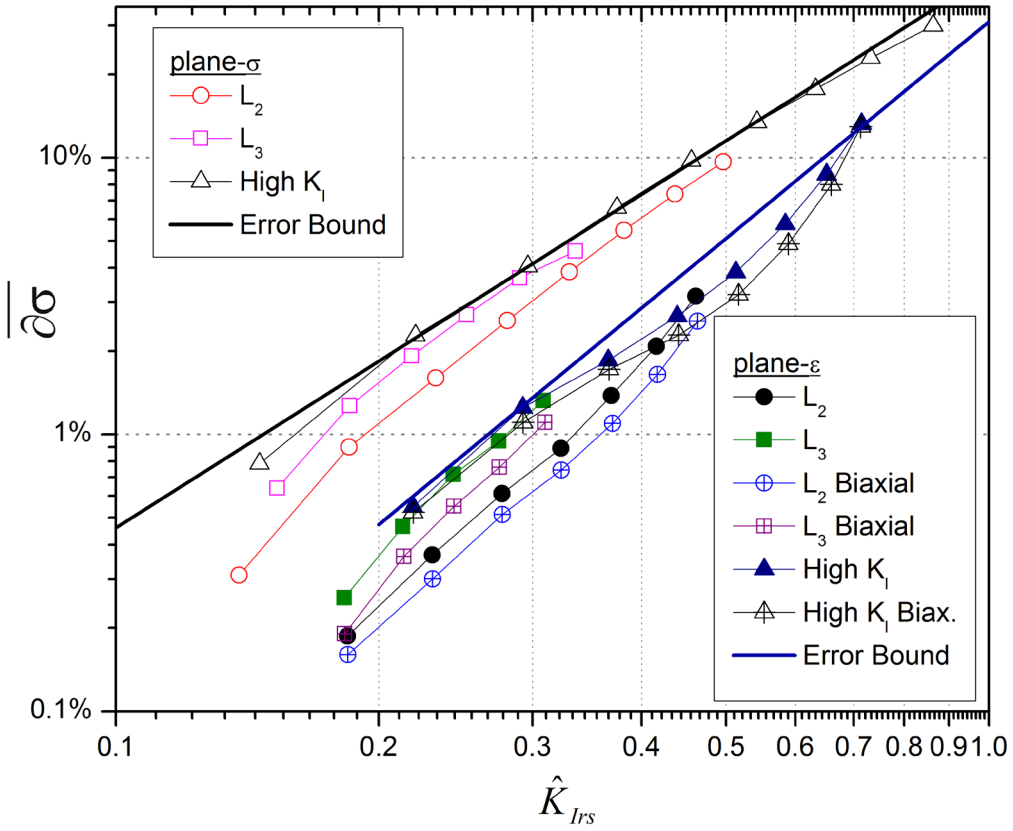

Figure 11. Logarithmic plot of stress errors and functions representing upper bounds to errors.

Figure 12 shows the maximum stress error for the 2-D parameter study. The maximum errors always occurred at the value nearest $x = 0$, which is at $x = a_1$, $0.01t$ in this case. The maximum errors would be greater if results were extrapolated to the surface and less if coarse cut depth increments were used. Therefore, the specific values are not as universally representative of all slitting measurements as the average values of Figure 9 are. In fact, $0.01t$ in, corresponds to nearly 100 cut depth increments which significantly exceed common practice of using something like 20 to 40 increments.

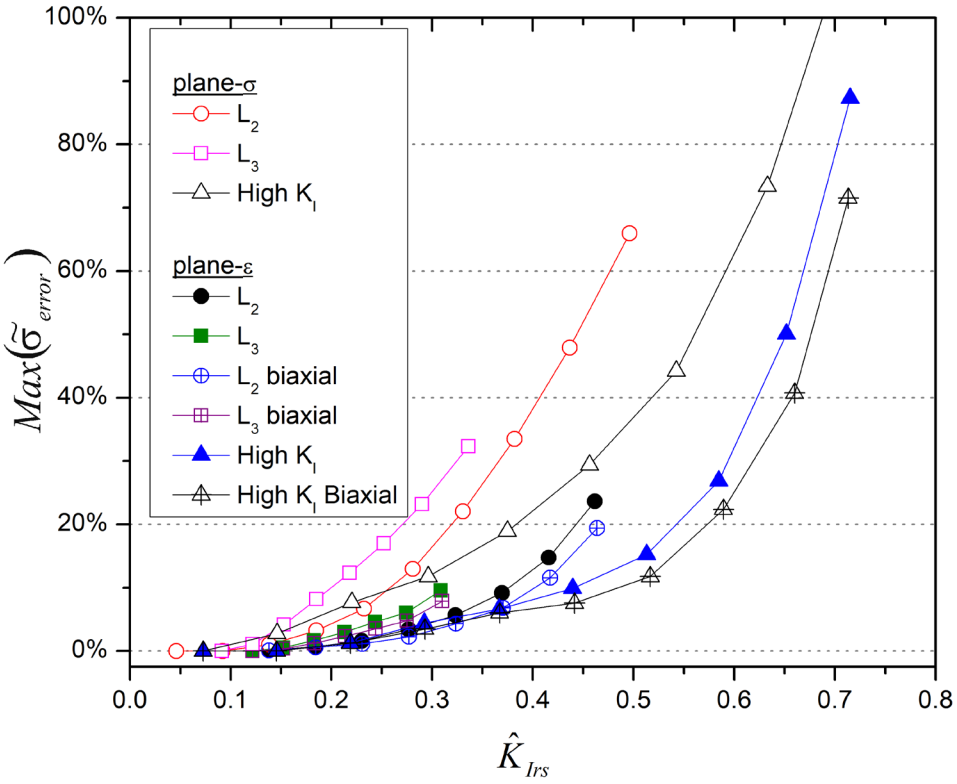

Figure 12. Maximum stress errors as a function of maximum in the apparent stress intensity factor.

Although the maximum stress errors are not as deterministic as the average errors, some useful observations are possible. At the same values that the average stress errors exceed 1%, the maximum errors hit about 5%. After the maximum stress errors reach about 20%, when $\hat{K}_{Irs}$ exceeds about 0.27 for plane stress or 0.44 for plane strain, the errors increase rapidly. For the plane stress simulation with the high K_{Irs} profile and a maximum stress of $0.5S_y$, the maximum calculated stress is $0.6S_y$, and the peak and average stress errors are about 20% and 6.5% respectively. All higher errors in the 2-D study have a higher calculated stress magnitude. Therefore, one probably does not need to consider plasticity error if the calculated stresses do not exceed $0.5S_y$ or $0.6S_y$.

3.4. 3-D results

A small set of computationally intensive 3-D FE runs were used to answer the most important questions posed by the 2-D results. The difference between the 2-D plane stress and plane strain results show that degree of constraint has a factor of three to four effect on the errors caused by plasticity. Therefore, it was necessary to determine where between plane stress (width = 0) and plane strain (infinite width) solutions a beam with finite width would fall. The L_2 and high K_{Irs} profiles were considered in the 3-D study. Uniaxial stresses were considered since biaxiality had little effect. Peak stress levels of 60% and 80% of the yield strength were considered in order to examine a reasonable range of errors in the measured stress results.

Figure 13 shows the most relevant results from the simulations for L_2 at 80% of the yield strength. The normalized difference between the strains with and without plasticity, Eq. 8, is plotted. The results show that as the specimen width increases, the difference strains more closely approximate the 2-D plane strain results. The 3-D results for the narrowest simulation, $W = 0.1t$, fall about half way between the plane strain and plane stress solutions. These results indicate that results based solely on plane stress simulations [23] will generally over-predict plasticity effects. The results for $r = 0.6$ are qualitatively similar.

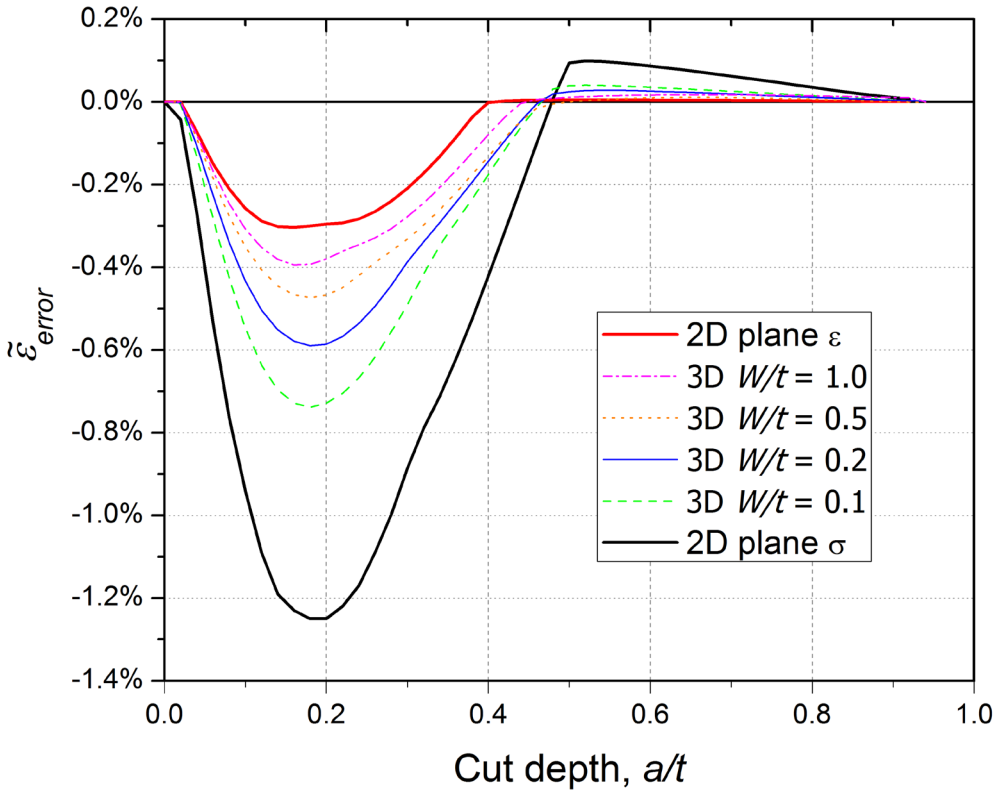

Figure 13. Plasticity effects from 3-D simulations for L_2 and $\sigma_{max} = 0.8\ S_y$ and various specimen widths compared to 2-D results.

A simple scalar measure is used to quantify where a 3-D results falls between the 2-D limiting cases. Since the shapes of the curves in Figure 13 are essentially similar, the peak magnitude of the curve, $\varepsilon^* = \max\left|\varepsilon_{plastic}(a) - \varepsilon_{elastic}(a)\right|$, can be used to approximately scale the results. Degree of plane strain is then defined as

$$D = \frac{\varepsilon^*_{3D} - \varepsilon^*_{p\sigma}}{\varepsilon^*_{p\varepsilon} - \varepsilon^*_{p\sigma}} \tag{14}$$

where the subscripts $p\sigma$ and $p\varepsilon$ refer to plane stress and plane strain, respectively. D is zero for plane stress and one for plane strain. This definition is analogous to the $\lambda = \sigma_z / \left[\nu\left(\sigma_x + \sigma_y\right)\right]$ degree of plane strain definition used in fracture mechanics.

Figure 14 plots the degree of plane strain for the 3-D finite element simulations. In terms of the effect of plasticity on slitting measurements, the 3-D result is better approximated by plane strain as compared to plane stress for all but the narrowest specimens. As the stress level increases, the size of the crack tip plastic zone relative to the specimen thickness increases, and the result becomes somewhat less plane strain [45].

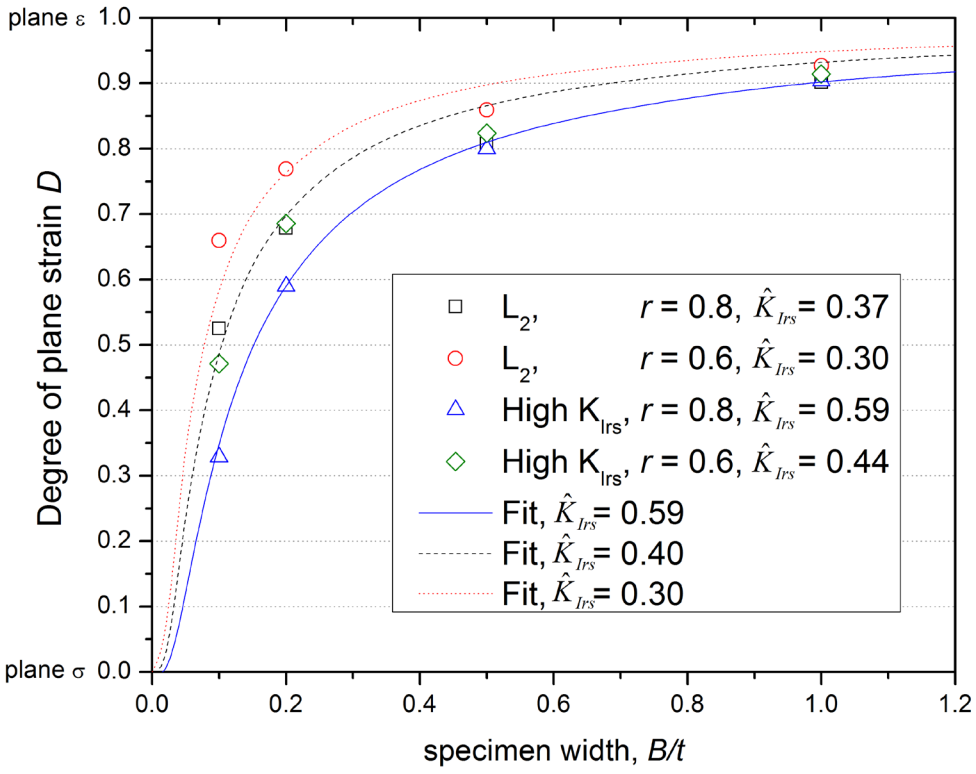

Figure 14. "Degree of plane strain" relevant to plasticity for different specimen widths and different stress levels.

3.5. 3-D/2-D interpolated results

The 3-D results of Figure 14 are used to interpolate the 2-D plane stress and plane strain results from Figure 10 to different specimen widths. For purposes of this interpolation, the results of Figure 14 can be fit to acceptable accuracy by

$$D = e^{-0.18\frac{\hat{K}_{Irs}}{B/t}}, \tag{15}$$

which is used to linearly interpolate the 2D bounding curves results to give an error bound of

$$\overline{\partial\sigma} = 0.46\left(\hat{K}_{Irs}\right)^2 + \mathrm{D}\left[0.31\left(\hat{K}_{Irs}\right)^{2.6} - 0.46\left(\hat{K}_{Irs}\right)^2\right] \tag{16}$$

This bound is plotted in Figure 15. Considering the conservatism in the fits in Figure 11, especially for plane strain, the errors are conservative. The errors start becoming significant for $\hat{K}_{Irs}$ exceeding 0.3 to 0.4 depending on the specimen width.

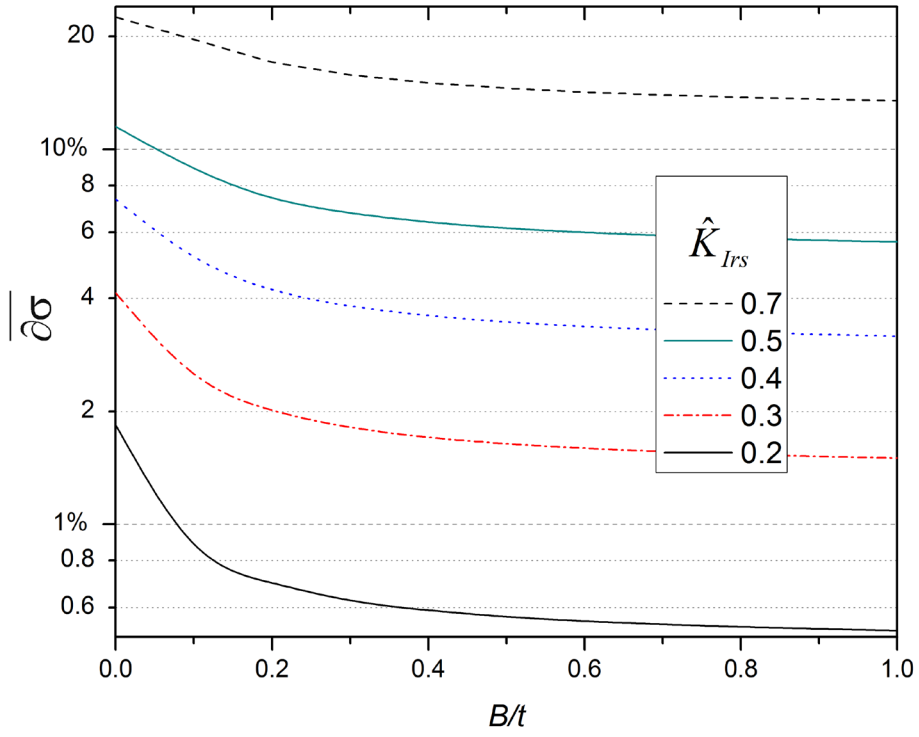

Figure 15. Average stress error as function of specimen width and magnitude of apparent stress intensity factor.

The literature was extensively examined for slitting tests that might cause plasticity errors. Such situations are unusual, but some are found in the literature in thin specimens. The specimens most likely to yield are from tests in friction stir welded aluminum alloys where the apparent $\hat{K}_{Irs}$ values were both over 0.3 and the *B/t* values were 0.05 and 0.15 [46, 47]. Figure 15 would indicate average errors of up to 6% and peak errors might exceed 20%. However, in both cases, the finite slit width and likely strain hardening would reduce the errors. Indeed, if plasticity errors had occurred in [46], the stress profile would probably not have been so symmetric since the $K_{Irs}(a)$ was very asymmetric, with significant magnitudes only before the midpoint like Figure 4, and Figure 7 indicates that the error would have been asymmetric. Laser peening stresses were measured in a thin titanium strip and calculated stresses were near in magnitude to the yield strength [48]. That data is not analyzed here for $\hat{K}_{Irs}$ since a different strain gauge location was used.

4. Conclusions

These conclusions apply to through-thickness slitting measurements on a beam using a strain gauge opposite the cut. Other geometries would be expected to give somewhat different errors, and a strain gauge location on the top surface near the cut might give very different errors. The results also might be different if a different method than series expansion was used to calculate the stresses from strain data. This study's conclusions about plasticity errors are generally conservative. Such likely occurrences as strain hardening or a finite-width and round-bottomed slot would lead to lower plasticity errors. The mitigating effect of strain hardening can be qualitatively assessed by

comparing with hole drilling studies that show the effect of even modest strain hardening to be quite significant in reducing errors [28]. The following conclusions are made:

- The majority of plasticity errors in slitting measurements come from plasticity near the cut tip.
- Yielding under the strain gauge on the back face can occur for stress distributions with oppositely signed stresses on the top and bottom surfaces, but is very unlikely.
- Plasticity errors can be estimated *without knowing the actual residual stresses* by using the strain data to calculate the apparent $K_{Irs}(a)$ and then comparing with the values in Figure 15 or Equations 15 and 16.
- Unlike hole drilling, the slitting method errors cannot be deterministically correlated with stress magnitude. When the calculated stresses do not exceed about $0.5S_y$, it can be safely assumed that the plasticity errors are insignificant and calculating $K_{Irs}(a)$ is not necessary. However, calculated stresses as high as S_y may be quite accurate if the stress distribution is one that does not results in a high $K_{Irs}(a)$.
- The errors are strongly affected by constraint, and plane strain is a better 2D approximation than plane stress for all but the narrowest specimens.
- For specimens wider than $0.5t$, the maximum K_{Irs} must exceed $0.4S_y\sqrt{t}$ for average stress errors to exceed 4%.
- Maximum stress errors are more difficult to predict than average errors because they depend on more factors. For the cases in this study, they range from four to seven times the average error.

- Because of the correlation with $K_{Irs}(a)$, the plasticity errors could potentially be corrected using the cut-depth adjustment approach proposed by Schindler [21] with an appropriate scale factor. An experimental correction [49] is probably not possible for slitting.

Much future work is possible to improve the fidelity of this study. One could investigate the effects of strain hardening, slit width and the shape of the cut tip. One could investigate other strain gauge locations and other inverse methods for calculating the stress from the strain data.

5. Acknowledgements

The author would like to thank several members of ASTM Task Group E28.13.02 for helpful discussions: Weili Cheng, C. Can Aydiner, Michael R. Hill, and Hans-Jakob Schindler. This work was performed at Los Alamos National Laboratory, operated by the Los Alamos National Security, LLC for the National Nuclear Security Administration of the U.S. Department of Energy under contract DE-AC52-06NA25396.

6. References

[1] Cheng W, Finnie I. Residual Stress Measurement and the Slitting Method. New York, NY, USA: Springer Science+Business Media, LLC, 2007.
[2] Cheng W, Finnie I, Gremaud M, Rosselet A, Streit RD. The compliance method for measurement of near surface residual stresses-application and validation for surface treatment by laser and shot-peening. Journal of Engineering Materials and Technology. 1994;116(4):556-560.
[3] Kang KJ, Yao N, He MY, Evans AG. A method for in situ measurement of the residual stress in thin films by using the focused ion beam. Thin Solid Films. 2003;443(1/2):71-77.
[4] Prime MB, Hill MR. Measurement of Fiber-Scale Residual Stress Variation in a Metal-Matrix Composite. Journal of Composite Materials. 2004;38(23):2079-2095.

[5] Sabate N, Vogel D, Gollhardt A, Keller J, Cane C, Gracia I, Morante JR, Michel B. Measurement of residual stress by slot milling with focused ion-beam equipment. Journal of Micromechanics and Microengineering. 2006;16(2):254-259.
[6] Cheng W, Finnie I. Measurement of residual stress distributions near the toe of an attachment welded on a plate using the crack compliance method. Engineering Fracture Mechanics. 1993;46(1):79-91.
[7] Prime MB, Hill MR. Residual stress, stress relief, and inhomogeneity in aluminum plate. Scripta Materialia. 2002;46(1):77-82.
[8] Aydiner CC, Ustundag E, Prime MB, Peker A. Modeling and measurement of residual stresses in a bulk metallic glass plate. Journal of Non-Crystalline Solids. 2003;316(1):82-95.
[9] Dalle Donna C, Lima E, Wegner J, Pyzalla A, Buslaps T. Investigations on Residual Stresses in Friction Stir Welds. 3nd International Symposium on Friction Stir Welding, 27 and 28 September 2001. Kobe, Japan: The Welding Institute TWI, UK; 2001. p. pdf/CDrom.
[10] Wang QC, Hu XD, Li W, Yuan JL. Numerical simulation of machining distortion of residually stressed aircraft aluminum components. Key Engineering Materials. 2006;315/316:235-238.
[11] Aydiner CC, Ustundag E. Residual stresses in a bulk metallic glass cylinder induced by thermal tempering. Mechanics of Materials. 2004;37(1):201-212.
[12] DeWald AT, Rankin JE, Hill MR, Schaffers KI. An improved cutting plan for removing laser amplifier slabs from Yb:S-FAP single crystals using residual stress measurement and finite element modeling. Journal of Crystal Growth. 2004;265(3/4):627-641.
[13] Kim BS, Bernet N, Sunderland P, Manson JA. Numerical analysis of the dimensional stability of thermoplastic composites using a thermoviscoelastic approach. Journal of Composite Materials. 2002;36(20):2389-2403.
[14] Prime MB, Prantil VC, Rangaswamy P, Garcia FP. Residual stress measurement and prediction in a hardened steel ring. Materials Science Forum. 2000;347-349:223-228.
[15] Hill MR, Lin WY. Residual stress measurement in a ceramic-metallic graded material. Journal of Engineering Materials and Technology. 2002;124(2):185-191.
[16] Finnie S, Cheng W, Finnie I, Drezet JM, Gremaud M. The computation and measurement of residual stresses in laser deposited layers. Journal of Engineering Materials and Technology. 2003;125(3):302-308.
[17] Chung TJ, Neubrand A, Rodel J. Effect of residual stress on the fracture toughness of Al2O3/Al gradient materials. Key Engineering Materials. 2002;206-2:965-968.
[18] Ersoy N, Vardar O. Measurement of residual stresses in layered composites by compliance method. Journal of Composite Materials. 2000;34(7):575-598.
[19] ASTM standard E 837–08. Standard Test Method for Determining Residual Stresses by the Hole-Drilling Strain-Gage Method: ASTM International; 2008.
[20] Schindler HJ, Finnie I. Determination of residual stresses and the resulting stress intensity factors in the ligament of pre-cracked plates. In: Karihaloo BL, Mai YW, Ripley MI, Ritchie RO, editors. 9th International Conference in Fracture (ICF9); April 1-5, 1997. Sydney, Australia: PERGAMON PRESS LTD; 1997. p. 523-530.

[21] Schindler HJ. Residual stress measurement in cracked components: capabilities and limitations of the cut compliance method. Materials Science Forum. 2000;347-349:150-155.
[22] Lee MJ, Hill MR. Intralaboratory repeatability of residual stress determined by the slitting method. Experimental Mechanics. 2007;47(6):745-752.
[23] Petrucci G, Zuccarello B. Effect of plasticity on the residual stress measurement using the groove method. Strain. 1996;32(3):97-103.
[24] de Swardt RR. Finite element simulation of crack compliance experiments to measure residual stresses in thick-walled cylinders. Journal of Pressure Vessel Technology. 2003;125(3):305-308.
[25] Venter AM, de Swardt RR, Kyriacou S. Comparative measurements on autofrettaged cylinders with large Bauschinger reverse yielding zones. Journal of Strain Analysis for Engineering Design. 2000;35(6):459-469.
[26] Beghini M, Bertini L, Raffaelli P. Numerical analysis of plasticity effects in the hole-drilling residual stress measurement. Journal of Testing and Evaluation. 1994;22(6):522-529.
[27] Beghini M, Bertini L, Raffaelli P. An account of plasticity in the hole-drilling method of residual stress measurement. Journal of Strain Analysis for Engineering Design. 1995;30(3):227-233.
[28] Beghini M, Bertini L. Recent advances in the hole drilling method for residual stress measurement. Journal of Materials Engineering and Performance. 1998;7(2):163-172.
[29] Gibmeier J, Kornmeier M, Scholtes B. Plastic deformation during application of the hole-drilling method. Materials Science Forum. 2000;347/349:131-136.
[30] Moharami R, Sattari-Far I. Experimental and numerical study of measuring high welding residual stresses by using the blind-hole-drilling technique. Journal of Strain Analysis for Engineering Design. 2008;43(3):141-148.
[31] Popelar CH, Barber T, Groom J. A METHOD FOR DETERMINING RESIDUAL-STRESSES IN PIPES. Journal of Pressure Vessel Technology. 1982;104(3):223-228.
[32] Cheng W, Finnie I. A method for measurement of axisymmetric axial residual stresses in circumferentially welded thin-walled cylinders. Journal of Engineering Materials and Technology. 1985;107(3):181-185.
[33] Prime MB, Hill MR. Uncertainty, Model Error, and Order Selection for Series-Expanded, Residual-Stress Inverse Solutions. Journal of Engineering Materials and Technology. 2006;128(2):175-185.
[34] Smith DJ, Bouchard PJ, George D. Measurement and prediction of residual stresses in thick-section steel welds. Journal of Strain Analysis for Engineering Design. 2000;35(4):287-305.
[35] Dong P. On the Mechanics of Residual Stresses in Girth Welds. Journal of Pressure Vessel Technology. 2007;129(3):345-354.
[36] Schajer GS. Application of finite element calculations to residual stress measurements. Journal of Engineering Materials and Technology. 1981;103(2):157-163.
[37] ABAQUS. Pawtucket, RI, USA: ABAQUS, inc.; 2003.

[38] Nervi S, Szabó BA. On the estimation of residual stresses by the crack compliance method. Computer Methods in Applied Mechanics and Engineering 2007;196(37-40):3577-3584.
[39] Schajer GS. Use of Displacement Data to Calculate Strain Gauge Response in Non-Uniform Strain Fields. Strain. 1993;29(1):9-13.
[40] Fett T, Munz D. Stress Intensity Factors and Weight Functions. Billerica, MA, USA: Computational Mechanics, Inc., 1997.
[41] Schindler HJ. Determination of residual stress distributions from measured stress intensity factors. International Journal of Fracture. 1990;74(2):R23-R30.
[42] Schindler HJ, Cheng W, Finnie I. Experimental determination of stress intensity factors due to residual stresses. Experimental Mechanics. 1997;37(3):272-277.
[43] Schindler HJ. Personal communication. 2007.
[44] Prime MB. Measuring residual stress and the resulting stress intensity factor in compact tension specimens. Fatigue & Fracture of Engineering Materials & Structures. 1999;22(3):195-204.
[45] Nakamura T, Parks DM. Three-dimensional crack front fields in a thin ductile plate. Journal of the Mechanics and Physics of Solids. 1990;38(6):787-812.
[46] Pouget G, Reynolds AP. Residual stress and microstructure effects on fatigue crack growth in AA2050 friction stir welds. International Journal of Fatigue. 2008;30(3):463-472.
[47] Milan MT, Bose WW, Ruckert COFT, Tarpani JR. Fatigue behaviour of friction stir welded AA2024-T3 alloy: longitudinal and transverse crack growth. Fatigue & Fracture of Engineering Materials & Structures. 2008;31(7):526-538.
[48] Rankin JE, Hill MR. Measurement of thickness-average residual stress near the edge of a thin laser peened strip. Journal of Engineering Materials and Technology. 2003;125(3):283-293.
[49] Mahmoudi AH, Hossain S, Truman CE, Smith DJ, Pavier MJ. A New Procedure to Measure Near Yield Residual Stresses Using the Deep Hole Drilling Technique. Experimental Mechanics. 2009;49(4):595-604.